Kulyakhtin, Sergey; Polojärvi, Arttu

Variation of stress in virtual biaxial compression test of ice rubble

Published in:
Proceedings of the 24th International Conference on Port and Ocean Engineering under Arctic Conditions, POAC'17

Published: 01/01/2017

Document Version
Publisher's PDF, also known as Version of record

Please cite the original version:
Kulyakhtin, S., & Polojärvi, A. (2017). Variation of stress in virtual biaxial compression test of ice rubble. In Proceedings of the 24th International Conference on Port and Ocean Engineering under Arctic Conditions, POAC'17 (Proceedings : International Conference on Port and Ocean Engineering Under Arctic Conditions). POAC. Proceedings of the International Conference on Port and Ocean Engineering under Arctic Conditions, POAC

POAC'17
Busan, KOREA

Proceedings of the 24th International Conference on
Port and Ocean Engineering under Arctic Conditions
June 11-16, 2017, Busan, Korea

Variation of Stress in Virtual Biaxial Compression Test of Ice Rubble

Sergey Kulyakhtin1 and Arttu Polojärvi[1,2]
[1] Sustainable Arctic Marine and Coastal Technology (SAMCoT), Centre for Research-based Innovation (CRI), Norwegian University of Science and Technology, Trondheim, Norway
[2] Aalto University, School of Engineering, Department of Mechanical Engineering
P.O. Box 14300, FI-00076 Aalto, Finland, e-mail: sergey.kulyakhtin@ntnu.no

ABSTRACT

Ice rubble constitutes ice ridges and rubble fields, which can exert high loads on offshore structures. To characterize the ice rubble, its average properties are often desired. The properties, such as, the critical state friction angle, rely on the continuum notion of stress. This study uses discrete element model for the ice rubble. We use an average stress tensor from the contact forces between the ice blocks and compare it to the macroscopic stress tensor yielded by the boundary contact forces. These stress definitions are used to evaluate the uncertainty in defining the stress tensor for the ice rubble, and the related uncertainty in defining the critical state friction angle for the rubble.

INTRODUCTION

To describe ice rubble properties in both natural and laboratory conditions, bulk parameters are often used. These parameters, such as the internal friction angle or cohesion (ISO, 2010), rely on the continuum notion of stress and displacement fields, or in other words, continuum approach. The ice rubble, however, is a granular material (consists of individual ice blocks), and it remains unclear, when the continuum approach can be applied for it. Here we will use the results from a 2D discrete element method (DEM) simulations of bi-axial compression tests on ice rubble, and study the error in the assumed stress state of a an ice rubble sample of given size.

The average stress tensor is a stress measure that can be applied for granular materials having a large number of individual particles. This is not necessarily the case for ice rubble, as an ice rubble sample of interest may only consist of tens, or hundreds, of ice blocks. Here we use a virtual bi-axial compression test on ice rubble to study the effect of averaging-volume size on the averaged stress tensor. First, we will describe the stress measures and the simulation set-up. Second, we will investigate how accurately the averaged stress tensor inside the sample represents the stress tensor derived from the boundary forces. We will also discuss the uncertainties in defining the critical state friction angle from the test results.

STRESS MEASURES

Several definitions for the averaged stress tensor for granular media exist. Here we use a definition that uses a weighting function. This allows us to vary the size of averaging volume independently of the configuration of the particles in the sample, which further allows us to study the applicability of the stress tensor itself on describing the stress state of rubble samples of various sizes. Babic (1997) defines such an average stress tensor $\bar{\sigma}$ at point x in the quasi-static case a

$$\bar{\sigma}_{ij} = \frac{1}{2}\sum_{\alpha}\sum_{\beta>\alpha} f_i^{\alpha\beta} x_j^{\alpha\beta} \int_0^1 w(\mathbf{x} - \mathbf{x}^{\alpha} + s\mathbf{x}^{\alpha\beta}, a)ds, \tag{1}$$

Where $f_i^{\alpha\beta}$ is the i^{th} component of the contact force between blocks α and β, $x_j^{\alpha\beta}$ is the j^{th} component of the vector $x^{\alpha\beta}$ connecting their centroids, w(x, a) is a weighting function, x^{α} is the position vector of the centroid of block α, and a is the side length of a square shaped AV. The above equation is not defined for the particles contacting the sample boundary, because it uses the distance between the centroids of blocks in contact (boundaries do not have one). For w(x, a), we use the Heaviside function that is normalized over a square domain

$$w(\mathbf{x}, a) = \left(\frac{1}{a^2}\right) H(a + x_i^0 - x_i)H(a + x_j^0 - x_j). \tag{2}$$

For equilibrium under uniform stress state, the average stress inside the sample can be always computed from the forces acting on the boundaries of the sample. These forces can be used to define a boundary stress tensor σ^b as (Drescher and de Josselin de Jong, 1972)

$$\sigma_{ij}^b = \frac{1}{V}\sum_{\alpha \in boundary} f_i^{\alpha} x_j^{\alpha}, \tag{3}$$

where V is sample volume and summation is over the sample boundary. In continuum sense, under uniform boundary conditions, the stress defined by Eq. 3 should be the same everywhere in the sample. Therefore, in our bi-axial compression tests, $\bar{\sigma}$ should be equal to σ^b, if the side length a of the averaging volume is large enough.

SIMULATION SET-UP

Our simulation tool has been validated against model- and full-scale experiments on ice-structure interaction in Paavilainen et al. (2009) and Paavilainen et al. (2011), respectively. In addition it was used to model laboratory scale shear box experiments on ice rubble in Polojärvi et al. (2015). In the model, the ice blocks are rigid and the contact forces are calculated using an elastic-viscous-plastic contact force model together with an incremental coulomb friction model (see Hopkins (1992) and Paavilainen et al. (2009) for details). Further, there is no cohesion between the blocks. The block fracture is not modelled. Table 1 gives the main parameters of the simulations.

Figures 1a and b illustrate the simulation set-up for our virtual biaxial compression experiment. All simulated samples consisted of 5000 uniformly sized blocks (block size was 0.3 x 0.9 m). We generated the initial configuration the figures illustrate by starting with a very loose and random blocks configuration, and by compressing it to an initial confinement $\sigma_{xx}^b = \sigma_{yy}^b =$ 5kPa. The boundaries were rigid and frictionless.

During the actual virtual compression experiments, the cover of the box moved downwards with a strain rate of $\dot{\epsilon}^b_{yy} = 5 \cdot 10^{-4} s^{-1}$ (we defined vertical component of the strain as $\epsilon^b_{yy} = \Delta h / h_0$ where Δh is the change in the specimen height and h0 is the initial height of the sample). Chosen strain rate was low enough to ensure a quasistatic loading as was indicated by the total load on the top and bottom of the box remaining virtually equal throughout the simulations. The location of the vertical boundaries was iterated on every simulation time step so that σ^b_{xx} remained constant. We used the confining stress $\sigma^b_{xx} = 5$kPa as it is an approximate average confinement on the top of a ten meters deep ridge keel (if continuous rubble mass is assumed). We ran simulations with five different ice block configurations to account for the potential effect of the initial ice rubble configuration.

RESULTS AND ANALYSIS

Boundary Stress

Figures 2a and b show the diagonal and off-diagonal components of the boundary stress σ^b (Eq. 3) as functions of strain ϵ^b_{yy}. The data in each figure are from five simulations with different initial configurations. Additionally, the figures show the mean of five records. As the figures show, σ^b_{xx} records are virtually equal to all configurations, but σ^b_{yy} records show some scatter. All configurations show similar behaviour: σ^b_{yy} first increases with high rate up to $\epsilon^b_{yy} \approx 0.01$, then continues to increase with slower rate, and finally reaches a plateau after $\epsilon^b_{yy} \approx 0.05$.

The off-diagonal stress components show random oscillations, while the mean value for different configurations is approximately zero (Figure 2b). The nonzero off-diagonal components are due to the external moments, which arise from the asymmetric boundary force distributions. To describe these stresses, the couple stress tensor, such as described in (Malvern, 1969), would be needed. This is however outside of the scope of this paper.

Table 1. Main simulation Parameters. Sample width and height depended on the initial configuration and confinement. Parameters were chosen as in Paavilainen et al. (2011)

Normal contact stiffness	4 GPa
Tangential contact stiffness	1.5 GPa
Normal damping factor	0.5
Tangential damping factor	0.25
Poisson coefficient	0.3
Bulk material density	900 kgm^{-3}
Plastic limit in contact (σ_p)	2 MPa
Ice-ice friction coefficient	0.3
Ice-boundary friction coefficient	0.0
Block length (l)	0.9 m
Block thickness	0.3 m
Initial sample width	≈40 m
Initial sample height (h_0)	≈40 m
Strain rate	$5 \cdot 10^{-4}$
Confining stress	5 kPPa

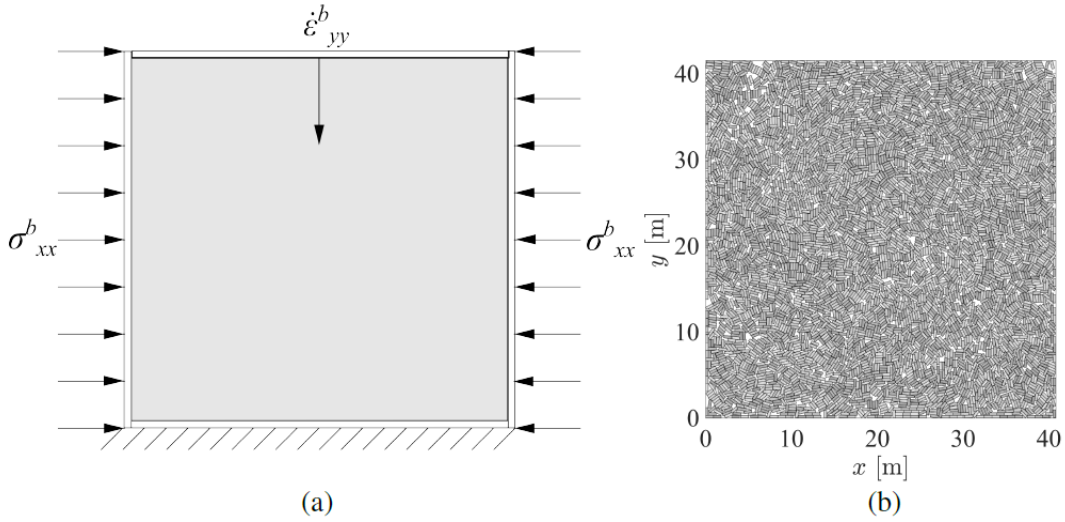

Figure 1. Virtual compression experiments: (a) simulation set-up and (b) a 5000 block sample in its initial configuration. The confining stress σ^b_{xx} was kept equal to 5 kPa and the cover moved down at the constant strain rate of $5\times10^{-4}s^{-1}$.

due to the external moments, which arise from the asymmetric boundary force distributions. To describe these stresses, the couple stress tensor, such as described in (Malvern, 1969), would be needed. This is however outside of the scope of this paper.

Convergence of averaged stress to boundary stress

In a continuum approximation, a uniform boundary stress imposes a uniform stress throughout the sample. This means that the average stress given by Eq. 1 should be equal to the boundary stress given by Eq. 3 at all material points of the sample. This will not hold if the averaging volume is small and only few blocks are used to compute $\bar{\sigma}$. However, $\bar{\sigma}$ should approach σ^b as the averaging volume size increases.

To study the convergence of $\bar{\sigma}$ we first chose to study the stress state of the sample at strain $\epsilon^b_{yy} = 0.15$ where the component σ^b_{yy} is approaching an approximately constant value. (We note that the stress $\bar{\sigma}$ can naturally be computed for any given strain.) Figures 3a and b show $\bar{\sigma}_{xx}$ and $\bar{\sigma}_{yy}$ values, which are here normalized by the corresponding boundary stress components, as a function of the averaging volume side length a divided by by the block length l. The figures clearly show that the diagonal components $\bar{\sigma}_{ii}$ of the average stress approach the corresponding components of σ^b_{ii}.

However, in some cases, the average stress for even the largest averaging volume differs by $>10\%$. This can be explained by non-uniform contact force distribution and the applicability of Eq. 1 and is described by Figure 4. The figure illustrates the contact force distributions for two samples at the initial state of the test $\epsilon_{yy} = 0$ (only initial confinement of 5 kPa) and at strain $\epsilon_{yy} = 0.15$ on its left and right columns, respectively. For clarity, only the forces that have a value of at least 20% of the maximum contact force are shown in each figure.

In both cases, the contact force distribution is seen to be initially uniform (left column of the figure). For the configuration in Figure 4a, the distribution also remains somewhat uniform up to $\epsilon = 0.15$, as the top right figure shows. The configuration in Figure 4b, however, has the

majority of the load carried by the blocks close to the left boundary at $\epsilon = 0.15$. The average stress $\bar{\sigma}$ (see Eq. 1) does not apply for these blocks, since they are in contact with the boundaries. This leads to σ not converging to σ^b. We studied the convergence of $\bar{\sigma}_{ij}$ for all time instances of our simulations, and found that about 7% of the cases behaved like this. As this behavior depends on the boundaries, these cases are excluded from the following analysis.

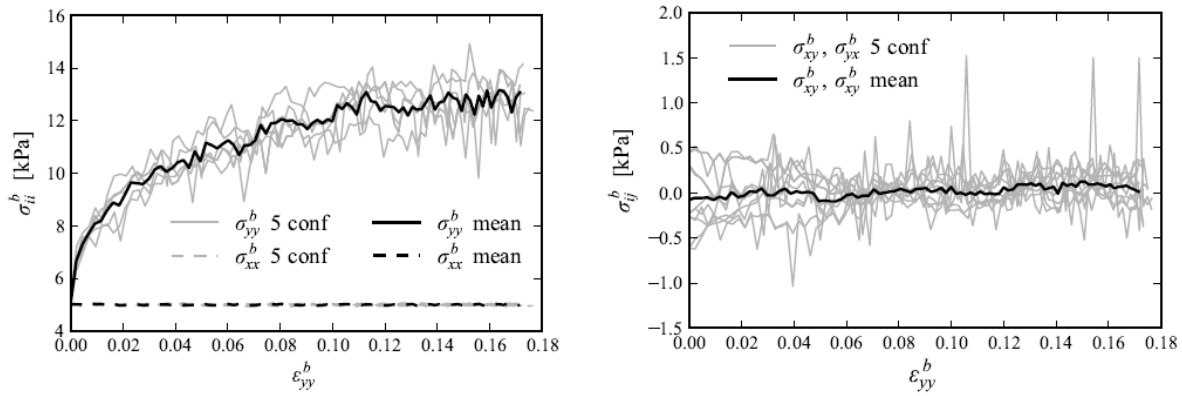

Figure 2. The diagonal (a) and off-diagonal (b) components of boundary stress tensor σ_{ij}^b as a function of strain ϵ_{yy}^b for five configurations and means of these configurations

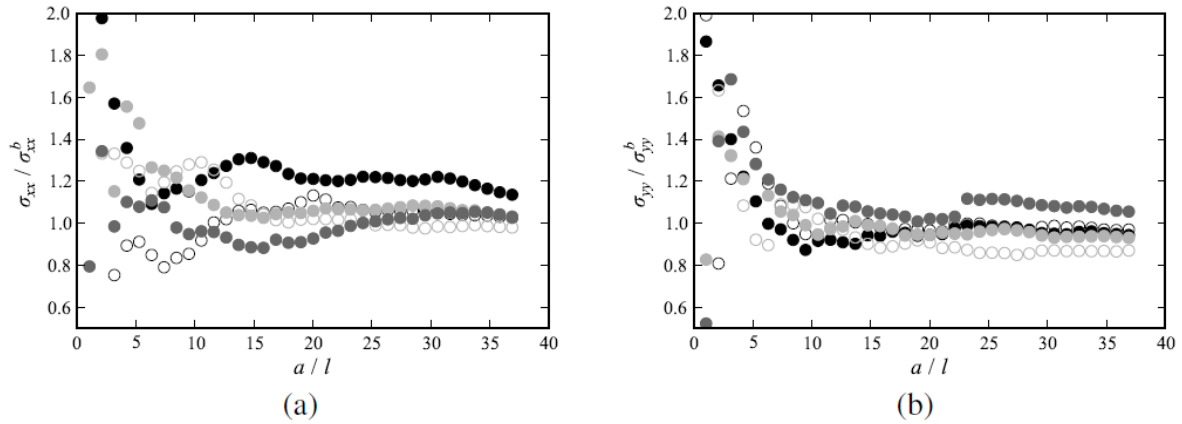

Figure 3. The diagonal stress components nomalised by the corresponding boundary stress components ($\bar{\sigma}_{ii}/\sigma_{ii}^b$) as a function of AV size normalised by block length (a/l) for five different configurations

We also calculated the $\bar{\sigma}_{ij}$ values for random points within our sample using a number of AV side lengths α. The aim in this study was two-fold: (1) to study the probability and the magnitude of error, if the sample size is chosen after some given value, and (2) to provide a proof-of-concept for the applicability of our approach on approximating the macroscopic stress state of the sample. In addition, the study indicates whether our analysis is sensitive to the choice of the stress averaging point. (Above, the $\bar{\sigma}_{ij}$ was always calculated at the center point of the sample.) We calculated $\bar{\sigma}_{ij}$ for 100 random points for all of our samples at every 0.01 strain increments.

Figures 5a and b show histograms that respectively illustrate the distribution of the normalised stresses $\bar{\sigma}_{xx}/\sigma_{xx}^b$ and $\bar{\sigma}_{yy}/\sigma_{yy}^b$ for random points of the sample. The histograms illustrate that

in all of the cases the normalized stress values are distributed around 1.0, and that their variation gets smaller as averaging volume size increases. The relative standard deviations for α = 5l are 28 % and 27 % for σ_{xx} and σ_{yy}, respectively. For averaging volumes having α = 20 l, the relative standard deviations are only 7 % and 9 % forσ_{xx} and σ_{yy}, respectively.

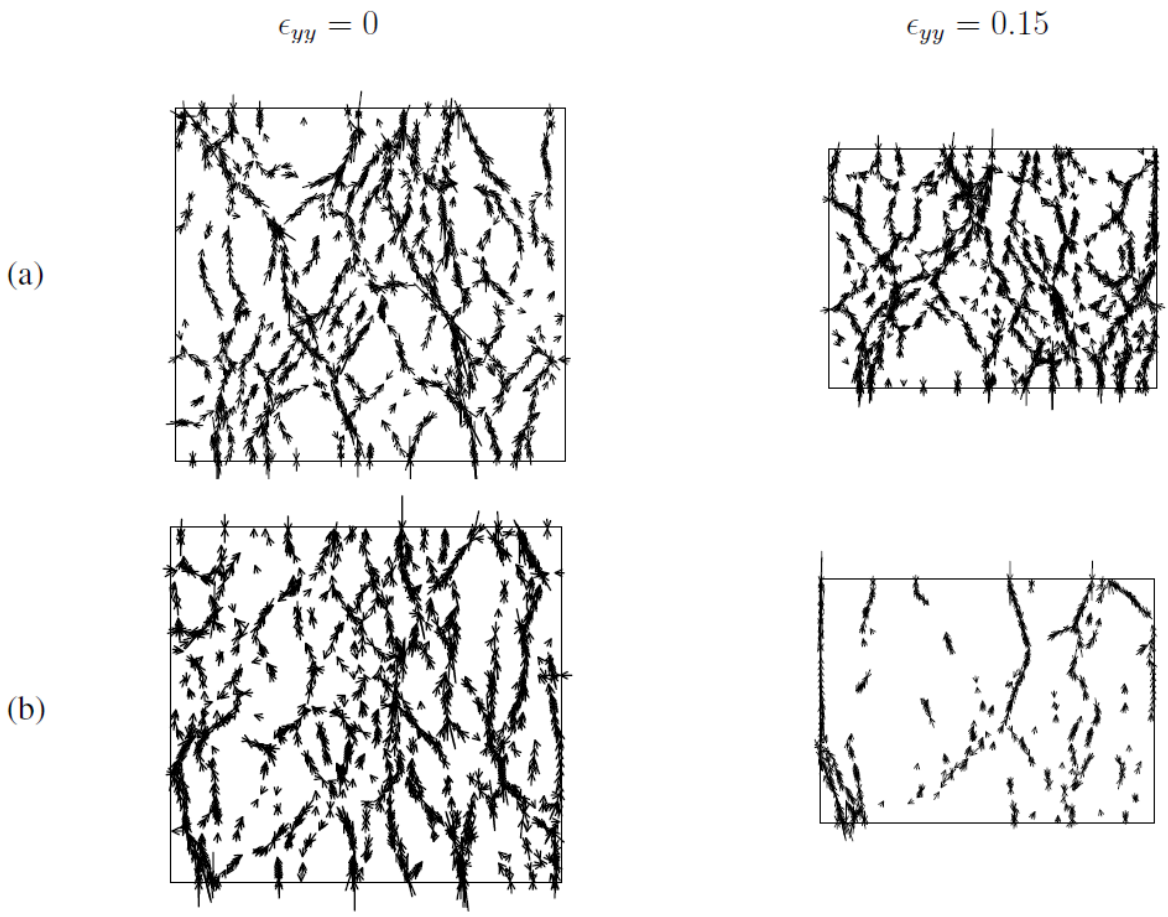

Figure 4. Two different initial configurations (a) and (b); and two instances of biaxial compression test $\varepsilon = 0$ and $\epsilon = 0.15$; the contact force vectors are shown that are ≥20% of the maximum contact force in the given instance

Variation in critical state friction angle

There is also uncertainty in the material parameters that are measured from the bi-axial test on insufficiently large sample. We demonstrate this by using the critical state friction angle ϕ_{cs} In the bi-axial compression test, ϕ_{cs} is calculated using the ratio of the major (here σ_{yy}) and minor (σ_{xx}) stress components as the ratio reaches a constant value (here this occurred at about ϵ = 0.15). The critical state friction angle is given by

$$\phi_{cs} = \arcsin\left(\frac{\sigma_{yy}/\sigma_{xx} - 1}{\sigma_{yy}/\sigma_{xx} + 1}\right). \quad (4)$$

Since there is a functional dependence of ϕ_{cs} on σ_{yy}/σ_{xx}, the relative standard deviation of the latter, std[σ_{yy}/σ_{xx}]/mean[σ_{yy}/σ_{xx}], can be used to calculate the relative standard deviation of ϕ_{cs}. This is given by

$$\frac{\mathrm{std}[\phi_{cs}(\sigma_{yy}/\sigma_{xx})]}{\phi_{cs}(\mathrm{mean}[\sigma_{yy}/\sigma_{xx}])} = \sqrt{\left(\frac{\partial\phi_{cs}}{\partial\left(\sigma_{yy}/\sigma_{xx}\right)}\bigg|_{\frac{\sigma_{yy}}{\sigma_{xx}}=\mathrm{mean}\left[\frac{\sigma_{yy}}{\sigma_{xx}}\right]}\right)^2}\frac{\mathrm{std}[\sigma_{yy}/\sigma_{xx}]}{\phi_{cs}(\mathrm{mean}[\sigma_{yy}/\sigma_{xx}])}$$
$$= \frac{1}{\sqrt{\mathrm{mean}[\sigma_{yy}/\sigma_{xx}]\,(\mathrm{mean}[\sigma_{yy}/\sigma_{xx}]+1)^2}}\frac{\mathrm{std}[\sigma_{yy}/\sigma_{xx}]}{\phi_{cs}(\mathrm{mean}[\sigma_{yy}/\sigma_{xx}])} \quad (5)$$

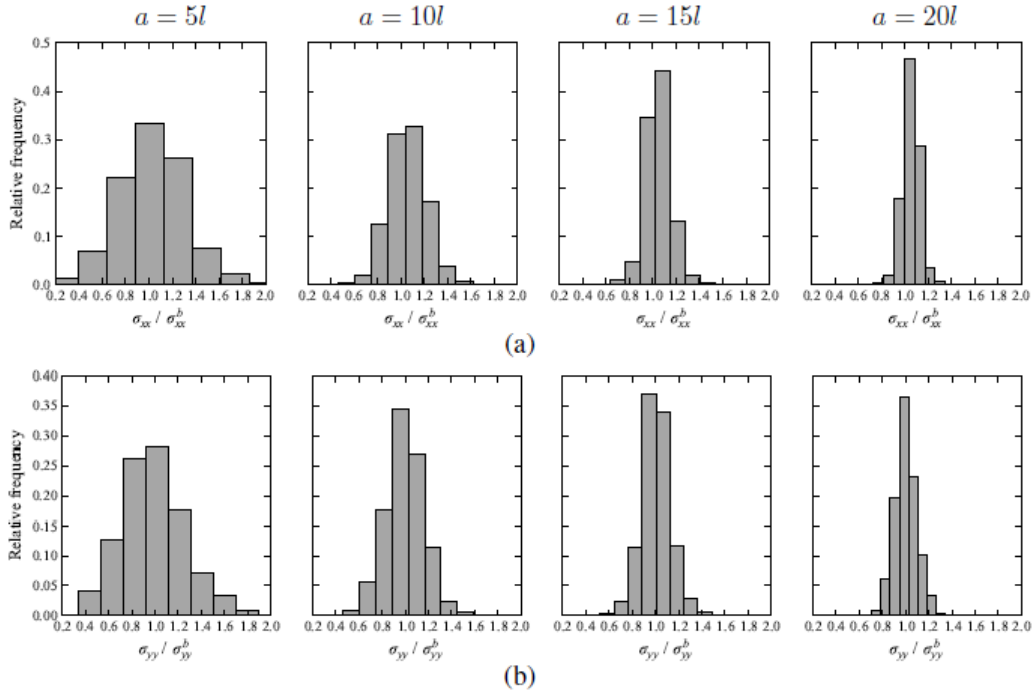

Figure 5. Histograms describing the distributions of the ratios of averaged stress to boundary stress ($\bar{\sigma}_{ij}/\sigma_{ij}^{b}$) calculated about 100 random points for all samples at intervals of 0.01 strain increment: graphs of (a) show $\bar{\sigma}_{xx}/\sigma_{xx}^{b}$ and (b) $\bar{\sigma}_{yy}/\sigma_{yy}^{b}$. The calculation was done using four different AV side lengths α (here a multiple of block length l) as indicated above each column.

We again computed the stress components in 100 random points to study the variation of σ_{yy}/σ_{xx} for averaging volumes of different sizes with the results shown in Figure 6. Here we only use data points with $\epsilon_{yy}^{b} \geq 0.15$, since only they should be used to compute ϕ_{cs} (approximately constant stress ratio was reached with $\epsilon_{yy}^{b} \geq 0.15$). The figure shows that, similarly to normalized stress, the variation in σ_{yy}/σ_{xx} gets continuously smaller as the averaging volume size increases.

Table 2. The relative standard deviations of the critical state friction angle ($\mathrm{std}[\phi_{cs}(\sigma_{yy}/\sigma_{xx})/\ \phi_{cs}(\mathrm{mean}[\sigma_{yy}/\sigma_{xx}])$]

	AV size			
	5 l	10 l	15 l	20 l
$\mathrm{std}[\phi_{cs}(\sigma_{yy}/\sigma_{xx})/\ \phi_{cs}(\mathrm{mean}[\sigma_{yy}/\sigma_{xx}])$	30%	18%	13%	10%

Table 2 summarises the relative standard deviations of ϕ_{cs} calculated by Eq. 5. These are 30% and 10% for the smallest (α/l=5) and largest (α/l= 20) averaging volumes, respectively, which is similar to the relative standard deviations of σ_{xx} and σ_{yy}. Table 2 also indicates that if a sample of only 10 block lengths is used to measure the critical state friction angle, even for the ice blocks with identical shape/size and properties, the variation in measured ϕ_{cs} of 18% should be expected.

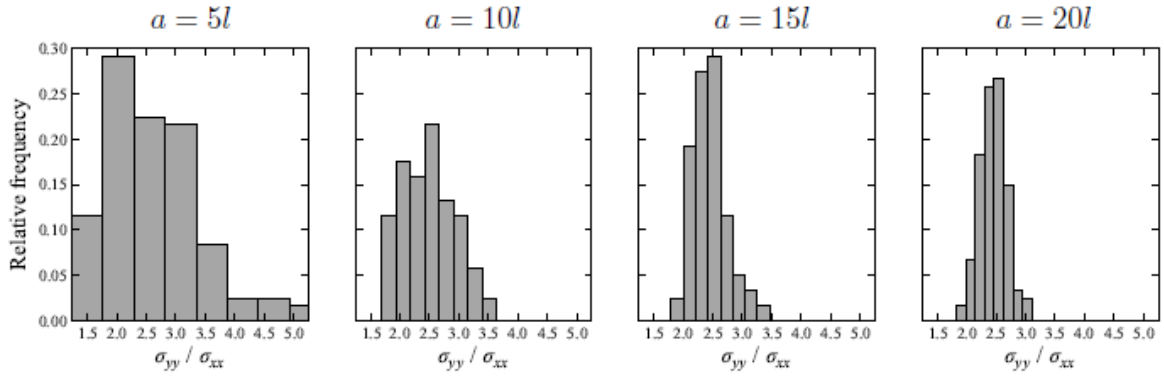

Figure 6. Histograms of σ_{xx}/σ_{yy} ratio computed in 100 random points for all samples at intervals of 0.01 strain increment starting from ϵ_{yy} = 0.15. The calculation was done using four different AV side lengths α (here a multiple of block length l) as indicated above each column.

CONCLUSIONS

We studied the applicability of the continuum approach in measuring the stress state of an ice rubble sample in bi-axial numerical experiment. Study was based on 2D DEM. The averaged stresses usually converged towards the boundary stress of the sample. In about 7% of cases this did not occur due to boundary conditions. For the rubble samples of size 5 block lengths, the ratio of averaged to boundary stress had a relative standard deviation of approximately 30%. This fell to about 10% with samples sizes of 20 block lengths. We also studied the effect of stress variation on the critical state friction angle. Its relative standard deviation was similar to those of the ratio of average to boundary stress.

ACKNOWLEGMENTS

The authors wish to acknowledge the support from the Research Council of Norway through the Centre for Research-based Innovation SAMCoT and the support from all SAMCoT partners.

REFERENCES

Babic, M. (1997). Average balance equations for granular materials. International journal of engineering science, 35:523–548.

Drescher, A. and de Josselin de Jong, G. (1972). Photoelastic verification of a mechanical model for the flow of a granular material. Journal of the Mechanics and Physics of Solids, 20(5):337–340.

Hopkins, M. (1992). Numerical simulation of systems of multitudinous polygonal blocks.

Technical
Report 92-22, Cold Regions Research and Engineering Laboratory, CRREL. 69 p.
ISO (2010). Petroleum and natural gas industries - Arctic offshore structures. Standard, International
Organization for Standardization, ISO 19906, Geneva, Switzerland.
Malvern, L. (1969). Introduction to the Mechanics of a Continuous Medium. Prentice-Hall, Inc.
Paavilainen, J., Tuhkuri, J., and Polojärvi, A. (2009). 2D combined finite–discrete element method to model multi-fracture of beam structures. Engineering Computations, 26(6):578–598.
Paavilainen, J., Tuhkuri, J., and Polojärvi, A. (2011). 2D numerical simulations of ice rubble formation process against an inclined structure. Cold Regions Science and Technology, 68(1-2):20–34.
Polojärvi, A., Pustogvar, A., and Tuhkuri, J. (2015). DEM simulations of direct shear box experiments
of ice rubble: Force chains and peak loads. Cold Regions Science and Technology, (116):12–23.